Transition to chaotic Taylor-Couette flow in shear-thinning fluids

S. A. BAHRANI[a], C. NOUAR[a], A. NEVEU[a] & S. BECKER[a]

a. LEMTA, UMR 7563 CNRS, Université de Lorraine, 2 Avenue de la Forêt de Haye, TSA 60604, Vandoeuvre lès Nancy F54518, France
seyed-amir.bahrani@univ-lorraine.fr & cherif.nouar@univ-lorraine.fr

Résumé :

Dans un article récent, Esmael et al. [1] ont étudié la transition vers la turbulence en conduite cylindrique pour un fluide non-Newtonien. Ils ont montré qu'une turbulence faible peut être générée par le caractère rhéofluidifiant du fluide. Un fluide rhéofluidifiant est un fluide dont la viscosité décroît non linéairement lorsque le cisaillement augmente. Dans la présente communication, nous confirmons ce résultat à travers une autre configuration géométrique. Nous présentons des résultats expérimentaux sur la stabilité d'un écoulement de Couette à large entrefer (rapport de rayons $\eta = R_1/R_2 = 0.4$) pour des solutions aqueuses de xanthan (fluide rhéofluidifiant et très faiblement élastique). Pour des concentrations suffisamment importantes, l'écoulement devient chaotique à partir de $Re = 1.5\ Re_c$ où Re_c est le nombre de Reynolds critique de bifurcation primaire. Pour un fluide Newtonien (solution de Glycérol), les tourbillons de Taylor restent stable jusqu'à $Re \approx 7.3 Re_c$ avant de bifurquer vers le régime ondulé. Une étude théorique basée sur des approches linéaire et faiblement non-linéaire est effectuée au préalable pour déterminer le nombre de Reynolds critique de bifurcation primaire ainsi que la nature de cette bifurcation.

Abstract :

In a recent paper, Esmael et al. [1] have studied the transition to turbulence in a pipe flow for non-Newtonian fluids. They have shown that a weak turbulence can be generated by the shear-thinning behavior of the fluid. A shear thinning fluid is a fluid for which the viscosity decreases non-linearly with increasing the shear rate. In this study, we confirm this result through a different geometrical configuration. We present experimental results on the stability of Couette flow with a wide gap (radius ratio $\eta = R_1/R_2 = 0.4$) for aqueous xanthan gum solutions (shear-thinning fluid and very weakly elastic). For sufficiently high concentrations, the flow becomes chaotic from $Re = 1.5\ Re_c$ where Re_c is the critical Reynolds number of the primary bifurcation. For a Newtonian fluid (glycerol solution), Taylor vortices remain stable up to $Re \approx 7.3 Re_c$ before bifurcating towards the wavy regime. A preliminary theoretical work based on linear and weakly nonlinear approaches is performed in order to determine the critical Reynolds number of the primary bifurcation as well as the nature of this bifurcation

Keywords : Taylor-Couette flow, shear-thinning fluids, stability.

1 Introduction

Taylor-Couette flow instabilities between two coaxial cylinders are considered as prototypes for general studies in hydrodynamic instability and transition to turbulence. In the classical configuration, the inner cylinder is rotating and the outer one is fixed. The primary instability occurs when the centrifugal force overcomes viscosity. Stationary counter-rotating vortices develop in the system via a supercritical bifurcation. Increasing the rotation of the inner cylinder above the critical value leads to a finite succession of the states before transition to a chaotic regime [2]. This transition to turbulence is governed by the Reynolds number (ratio between nonlinearity of the inertia terms and viscous dissipation terms). In the case of non-Newtonian fluids (polymer solutions, suspensions, emulsions, ...), mechanisms of the instability and transition to turbulence may be modified by the nonlinearity of the rheological behavior. Most non-Newtonian fluids have two common properties, viscoelasticity and shear-thinning. There was a significant interest in inertialess viscoelastic Taylor-Couette instability [3]. In the laminar state, the rotation produces a shear which stretches the polymer molecule along the curved stream lines. This leads to a first normal stress difference which acts against the centrifugal force. Groisman and Steinberg (1998) [4] showed experimentally that elastic instability leads to a strong nonlinear flow transition at vanishing inertia.

Hereafter, we focus on shear-thinning fluids, for which the elastic response can be neglected. The objective of the present work is to analyze the influence of the nonlinear variation of the viscosity with shear-rate on Taylor-Couette instabilities. We show on one hand that the nature of the bifurcation can be modified by shear-thinning effects and on the other hand, that a chaotic regime can be induced by the shear-thinning behavior.

2 Couette flow of a shear-thinning fluid

We consider the flow of a shear-thinning incompressible fluid between two infinitely coaxial cylinders of inner and outer radii $\hat{R}_1$ and $\hat{R}_2$ respectively. The radius ratio is $\eta = \hat{R}_1/\hat{R}_2$. The outer cylinder is at rest and the inner cylinder rotates with an angular velocity $\hat{\Omega}_1$. The governing equations in dimensionless form are :

$$\boldsymbol{\nabla} \cdot \mathbf{U} = 0 \tag{1}$$

$$\partial_t \mathbf{U} + Re(\mathbf{U} \cdot \boldsymbol{\nabla})\mathbf{U} = -\boldsymbol{\nabla} P + \boldsymbol{\nabla} \cdot \boldsymbol{\tau} \tag{2}$$

Here $\mathbf{U} = U\mathbf{e}_r + V\mathbf{e}_\theta + W\mathbf{e}_z$ is the velocity, P the pressure and $\boldsymbol{\tau}$ the deviatoric extra-stress tensor. The governing equations have been nondimensionalized using the annular gap $\hat{d} = \hat{R}_2 - \hat{R}_1$ as the reference length scale, the velocity of the inner cylinder $\hat{\Omega}_1\hat{R}_1$ as velocity scale, $\hat{\mu}_{ref}\hat{\Omega}_1\hat{R}_1/\hat{d}$ for stresses and pressure scale, viscous diffusion time $\hat{\rho}\ \hat{d}^2/\hat{\mu}_{ref}$ for time scale. The viscosity reference $\hat{\mu}_{ref}$ will be specified later. The Reynolds number Re is defined by :

$$Re = \hat{\rho}\hat{\Omega}_1\hat{R}_1\hat{d}/\hat{\mu}_{ref} \tag{3}$$

The quantities defined with a hat ($\hat{.}$) are dimensional, while quantities without ($\hat{.}$) are dimensionless. To the previous equations, we add the no-slip and impermeability condition at the walls :

$$\mathbf{U}(R_1) = (0, 1, 0) \quad \text{and} \quad \mathbf{U}(R_2) = 0 \tag{4}$$

The fluid is supposed to be purely viscous i.e. its viscosity depends only on the shear rate. The constitutive equation reads :

$$\boldsymbol{\tau} = \mu(\Gamma)\dot{\boldsymbol{\gamma}} \tag{5}$$

where, Γ is the second invariant of the strain-rate tensor $\dot{\boldsymbol{\gamma}}$. The viscosity μ is assumed to fit the power-law model :

$$\mu(\Gamma) = \Gamma^{\frac{n-1}{2}} \quad ; \quad \Gamma = \frac{1}{2}\dot{\gamma}_{ij}\dot{\gamma}_{ij} \tag{6}$$

where, $0 < n \leq 1$ is the shear-thinning index. The reference viscosity is :

$$\hat{\mu}_{ref} = \hat{K}\left(\frac{\hat{R}_1\hat{\Omega}_1}{\hat{d}}\right)^{n-1} \tag{7}$$

with $\hat{K}$ $[Pa.s^n]$, the fluid consistency.

2.1 Base flow

The base flow is purely azimuthal and is solution of :

$$\frac{d}{dr}(r^2\tau^b_{r\theta}) = 0 \tag{8}$$

with the boundary conditions

$$V^b(R_1) = 1 \quad ; \quad V^b(R_2) = 0 \tag{9}$$

The superscript "b" refers to the base flow. The velocity profile is given by :

$$V^b(r) = \frac{r}{R_1}\left[1 - \left(\frac{1}{R_2^{2/n}} - \frac{1}{R_1^{2/n}}\right)^{-1}\left(\frac{1}{r^{2/n}} - \frac{1}{R_1^{2/n}}\right)\right] \tag{10}$$

Figure $1a, b$ shows the effect of shear-thinning index on the velocity and viscosity profiles at $\eta = 0.4$. With increasing shear-thinning effects, the curvature of the velocity profile becomes more pronounced. The shear rate increases at the inner wall and decreases at the outer wall. The wider is the gap the more this effect is significant. This results in a viscosity stratification. The viscosity increases from the inner to the outer wall. As can be seen in figure $1b$, for $n = 0.2$, which corresponds practically to one of the fluids (0.5% wt xanthan gum) used in our experiments, the viscosity near the outer wall is 10^3 larger than that near the inner one.

2.2 Disturbance equations

The velocity **U** and the pressure P of the disturbed flow are splitted into the base field (with the superscript "b") and the disturbance :

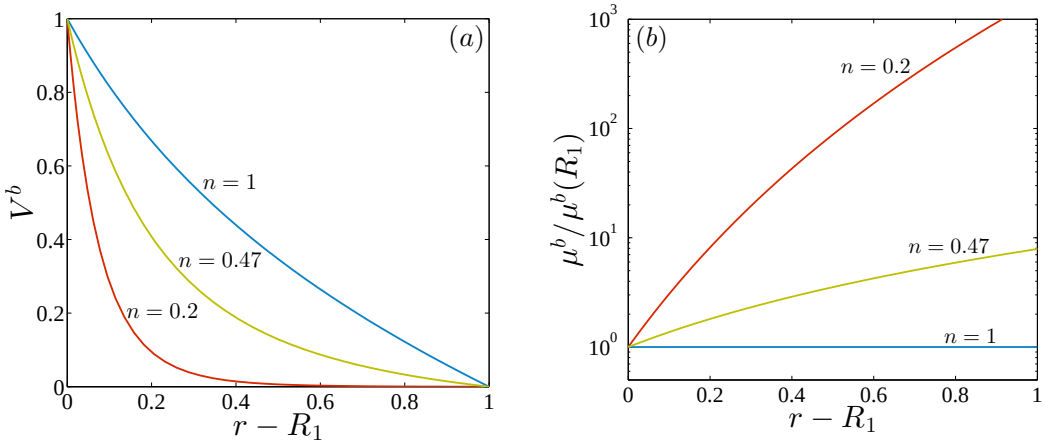

FIGURE 1: Couette flow of a power-law fluid at $\eta = 0.4$: (a) Azimuthal velocity and (b) Viscosity profiles.

$$\mathbf{U} = \mathbf{U}^b + \mathbf{u} \quad ; \quad P = P^b + p \tag{11}$$

Here, we consider only axisymmetric disturbances. These are the least stable modes when the outer cylinder is fixed as indicated by Alibenyahia et al. [5]. We introduce the function $\phi(r, z; t)$ such that :

$$u = -\frac{\partial \phi}{\partial z} \quad \text{and} \quad w = \left(\frac{\partial \phi}{\partial r} + \frac{\phi}{r}\right) \tag{12}$$

In axysimmetric situation, disturbance equations can be written in terms of the azimuthal vorticity ω_θ and the azimuthal velocity v :

$$\frac{\partial \omega_\theta}{\partial t} = Re\left[\frac{\partial \phi}{\partial z} D\omega_\theta - D^*\phi\frac{\partial \omega_\theta}{\partial z} + \frac{1}{r}\frac{\partial \phi}{\partial z}\omega_\theta - \frac{2v}{r}\frac{\partial v}{\partial z} - 2\frac{V^b}{r}\frac{\partial v}{\partial z}\right] + \left(DD^* - \frac{\partial^2}{\partial z^2}\right)\tau_{rz} + \frac{\partial}{\partial z}\left(D\tau_{zz} - D^*\tau_{rr}\right) + \frac{1}{r}\frac{\partial}{\partial z}\tau_{\theta\theta} \tag{13}$$

$$\frac{\partial v}{\partial t} = -Re\left[\frac{\partial \phi}{\partial z} D^* v - D^*\phi\frac{\partial v}{\partial z} + \frac{\partial \phi}{\partial z} D^* V^b\right] + \frac{1}{r^2}\frac{\partial}{\partial r}\left(r^2\tau_{r\theta}\right) + \frac{\partial}{\partial z}\tau_{\theta z} \tag{14}$$

where $\omega_\theta = \left(\frac{\partial^2}{\partial z^2} + DD^*\right)\phi$, $D \equiv \frac{\partial}{\partial r}$ and $D^* \equiv D + \frac{1}{r}$. The boundary conditions $\mathbf{u} = 0$ on R_1 and R_2 imply that :

$$\frac{\partial \phi}{\partial z} = D^*\phi = v = 0 \quad \text{on} \quad R_1 \quad \text{and} \quad R_2 \tag{15}$$

For a small amplitude disturbance, the viscosity of the perturbed flow can be expanded around the base flow as :

$$\mu(\mathbf{U}^b + \mathbf{u}) = \mu^b + \mu_1(\mathbf{u}) + \mu_2(\mathbf{u}, \mathbf{u}) + \mu_3(\mathbf{u}, \mathbf{u}, \mathbf{u}) + ... \tag{16}$$

The deviatoric stress in the disturbed flow can be written as :

$$\tau_{ij}(\mathbf{U}^b + \mathbf{u}) = \left(\mu^b + \mu_1(\mathbf{u}) + \mu_2(\mathbf{u},\mathbf{u}) + \mu_3(\mathbf{u},\mathbf{u},\mathbf{u}) + ...\right)\left(\dot{\gamma}^b_{ij} + \dot{\gamma}_{ij}(\mathbf{u})\right) \tag{17}$$

2.2.1 Linear stability analysis

The linearized version of the disturbance equations (13-14) can be written formally as :

$$\frac{\partial}{\partial t}\begin{bmatrix} DD^* + \dfrac{\partial^2}{\partial z^2} \\ 1 \end{bmatrix}\begin{bmatrix}\phi \\ v\end{bmatrix} = \mathcal{L}_I\begin{bmatrix}\phi \\ v\end{bmatrix} + \mathcal{L}_v\begin{bmatrix}\phi \\ v\end{bmatrix} \tag{18}$$

where $\mathcal{L}_I$ and $\mathcal{L}_v$ represent the linear inertial and viscous terms respectively. In a classical way, normal mode analysis is used, assuming that :

$$\begin{bmatrix}\phi \\ v\end{bmatrix} = \begin{bmatrix}F_{11}(r) \\ V_{11}(r)\end{bmatrix} e^{(ikz+ct)} \tag{19}$$

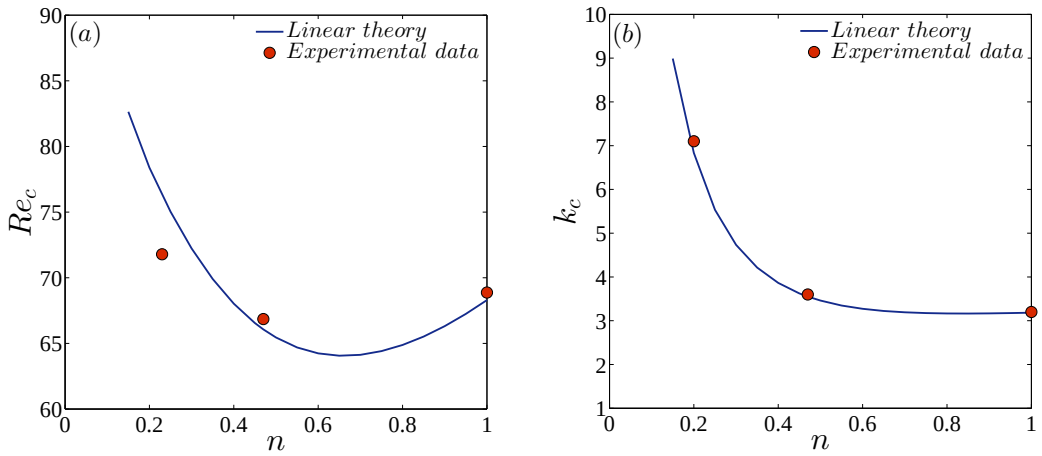

FIGURE 2: Comparison of theoretical (continuous line) and experimental (filled circle) variations of (a) the critical Reynolds number Re_c and (b) the axial wave number k_c as function of the shear-thinning effects n.

where k is the axial wave number and $c = c_r + ic_i$ is the complex wave speed. Substituting (19) into (18), we obtain an eigenvalue problem, which is solved using Chebyshev collocation method.

The influence of shear-thinning effects on the critical Reynolds number and axial wave number is shown in figure 2. One can note that k_c increases with increasing shear-thinning effects. At $n = 0.23$ the size of Taylor vortices is smaller than half that obtained for a Newtonian fluid.

2.2.2 Weakly nonlinear stability analysis

In the weakly nonlinear approach it is assumed that the solution of the nonlinear problem near the threshold bifurcation point can be approximated by a perturbation around the fundamental mode. Due to nonlinear terms, the fundamental interacts with itself, with its complex conjugate and with the mean flow which result in the generation of harmonics, a mean flow distortion and a modification of the fundamental respectively. The disturbance $\phi(r, z; t)$ is expanded as an amplitude and harmonic expansion :

$$\begin{bmatrix}\phi(r,z;t)\\ v(r,z;t)\end{bmatrix} = \sum_{n=1}\begin{bmatrix}F_{0,2n}(r)\\ V_{0,2n}(r)\end{bmatrix}|A|^{2n} + \sum_{j=1}\sum_{n=1}\begin{bmatrix}F_{i,j+2(n-1)}(r)\\ V_{i,j+2(n-1)}(r)\end{bmatrix}|A|^{2(n-1)}A^jE^j + c.c \tag{20}$$

In this equation, $c.c$ means the complex conjugate of the expression that precedes, E is the critical wave defined by $E \equiv exp[ikz + c_c t]$, with the critical wave numbers k_c, $A = A(t)$ is the complex amplitude of the fundamental. The time evolution of the disturbance amplitude A is given by the Stuart-Landau equation :

$$\frac{dA}{dt} = cA + g_1|A|^2A \tag{21}$$

The modulus of the amplitude A is determined by :

$$\frac{d|A|}{dt} = c_r|A| + g_{1r}|A|^3 \tag{22}$$

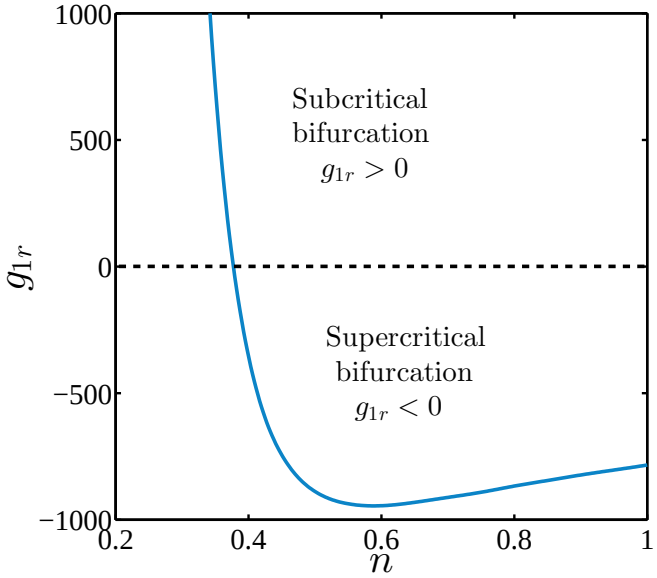

FIGURE 3: Evaluation of the real part of the Landau constant g_{1r} with a shear-thinning effects n

The nature of the bifurcation is determined by the real part g_{1r} of the Landau constant. If $g_{1r} < 0$ the bifurcation is supercritical and if $g_{1r} > 0$, the bifurcation is subcritical as can be shown in figure 3.

3 Experimental set-up and rheology of used fluid

The experimental system consists of two vertical coaxial cylinders. The outer cylinder (OC) is made of Plexiglas with a radius $\hat{R}_2 = 5\ cm$. The inner cylinder (IC) is made of stainless steel with a radius $\hat{R}_1 = 2\ cm$. The annular gap is $\hat{d} = \hat{R}_2 - \hat{R}_1 = 3\ cm$, with a radius ratio $\eta = \hat{R}_1/\hat{R}_2 = 0.4$. The aspect ratio (i.e. annulus length / gap width) is $\hat{h}/\hat{d} = 31$. The outer cylinder is kept at rest and the inner cylinder is driven by a DC servomotor. The working fluids used are : (i) a 80 wt% aqueous glycerol solution, which is Newtonian fluid, and (ii) two aqueous xanthan gum (semi-rigid polymer) solutions at 0.1 and 0.5 wt%. The rheological behavior of these solutions was determined using controlled torque

rheometer (TA Instrument AR2000). The variation of the shear viscosity $\hat{\mu}$ with the shear rate $\hat{\dot{\gamma}}$ is show in figure 4. For the xanthan gum solutions, the flow curves ($\hat{\mu}\ vs\ \hat{\dot{\gamma}}$) are very well fitted by the power-law model ($\hat{\mu} = \hat{K}\hat{\dot{\gamma}}^{n-1}$) for the whole range of shear rate encountered in our experiments.

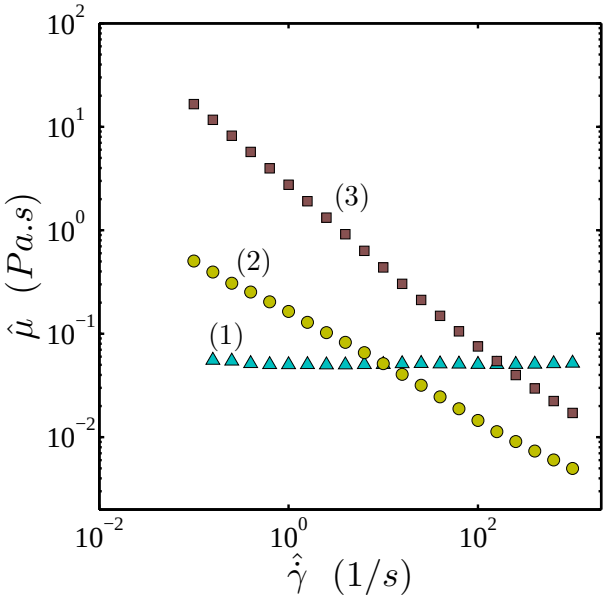

FIGURE 4: Viscosity vs shear rate : (1) 80 wt% glycerol solution, (2) 0.1 wt% xanthan gum solution $n = 0.47$ and (3) 0.5 wt% xanthan gum solution $n = 0.23$.

The Weissenberg number $Wi = N_1/\tau$, ratio of the first normal stress difference to the shear stress, is much lower than 1 ($Wi \ll 1$), therefore viscoelastic effects can be neglected. The temperature of the working fluids varies by no more than 0.8°C over the course of our experiment.

The evolution of the flow structure with increasing Reynolds number was determined from measurements of the velocity field by PIV and the space-time diagrams deducted from visualization. For this last purpose, the flow was seeded with a small amount of dilute solution of Merck IriodinÆ 110 (anisotropic mica platelets - particle size $< 15\mu m$). An $(r - z)$ plane is illuminated by He-Ne laser sheet (λ=532 nm, thickness 1.5 mm). A CCD camera (1200 $\times$ 1200 px) records the scattered intensity at 90°along an axial cross section of the entire cylinder.

4 Results and discussion

For the glycerol solution, the onset of centrifugal instability (TVF regime) takes place experimentally at Reynolds number $Re_c = 68.9$ with an axial wave number $k = 3.20$. These values match very well with the linear stability analysis. The velocity of rotation of the inner cylinder was increased progressively and slowly. As shown in figure 5c, up to $\approx 7.3 \times Re_c$, the Taylor vortices, separated by radial jets, remain stationary and axisymmetric. Their size (axial wavelength) does not vary. The pure singly periodic motion has been reported, in the case of wide gap $\eta = 0.505$, experimentally up to $9Re_c$ [8] and numerically up to $10Re_c$ [7]. These results are in agreement with stability analysis of Taylor vortices with respect to non-axisymmetric perturbations [6]. Increasing further $\hat{\Omega}_1$ (Re_1) the vortex flow becomes wavy and acquire another periodicity along θ. At a given azimuthal position the azimuthal periodicity is transported into a time periodicity (vortices moving up and down along the vertical axis) as shown in

figure 5d. This mode disappears at $\approx 8.5Re_c$, and the flow returns to the TVF state and remains in this state until a new wavy state is excited at $\approx 10.7Re_c$.

For 0.1 wt% xanthan gum solution, power-law fluid with $n = 0.47$, Taylor Vortex Flow (TVF) due to primary centrifugal instability is observed experimentally at $Re_c = 66.8$ with an axial wave number $k = 3.6$. These values are in a good agreement with the linear theory as indicated in figure 2. The rotation of the inner cylinder was then gradually increased. At $Re \approx 1.8\ Re_c$, the TVF regime looses its stability. Also, Taylor cells loose their identity. As Re increased further the flow becomes increasingly complex and chaotic.

For 0.5 wt% xanthan gum solution, power-law fluid with $n = 0.23$, the onset of centrifugal instability occurs slightly befor the linear theory prediction. *It could be viewed as a first experimental observation of a subcritical bifurcation in a Taylor-Couette system for shear-thinning fluids*. This is in agreement with the results of weakly nonlinear analysis (see figure 3). At $Re = 1.02\ Re_c$, Taylor vortices exhibit a drifting at approximately $1\ mm/s$, along the axis of the geometry in the direction opposite to the centerbody rotation vector. This observation is consistent with the description made by Escudier et al. (1995)[9]. At higher Re say $Re \geq 1.5\ Re_c$ a chaotic flow is observed.

In figure 6, we have represented the critical relative Reynolds number $\varepsilon_c = (Re - Re_c)/Re_c$ at which TVF looses its stability as a function of the shear-thinning index. It is observed that shear-thinning effects reduce strongly ε_c.

5 Conclusion

The stability of Newtonian and non-Newtonain shear-thinning in a wide gap Taylor-Couette system (radius rate $\eta = 0.4$) is investigated. For a Newtonain fluid, Taylor vortices are stable up to $Re \approx 7.3Re_c$ before bifurcating to a wavy regime. This mode disappears at $\approx 8.5Re_c$, and the flow returns to the TVF state and remains in this state until a new wavy state is excited at $\approx 10.7Re_c$. For xanthan gum solutions, shear-thinning fluids, the critical values of the relative Reynolds number ε_c at which Taylor vortices loose their stability decreases strongly with increasing shear-thinning effects. At $\varepsilon > \varepsilon_c$, the flow structure becomes increasingly complex and chaotic.

Références

[1] A. Esmael, C. Nouar, A. Lefèvre and N. Kabouya, Transitional flow of a non-Newtonian fluid in a pipe : Experimental evidence of weak turbulence induced by shear-thinning behavior, Phys. Fluids. **22** (2010) 101701.

[2] C. D. Andereck, S. S. Liu and H. L. Swinney, Flow regimes in a circular Couette system with independently rotating cylinders, J. Fluid Mech. **164** (1986) 155–183.

[3] G. Larson, E. S. G. Shaqfeh and S. J. Muller, A purely elastic instability in Taylor-Couette flow, J. Fluid Mech. **218** (1990) 573–600.

[4] A. Groisman and V. Steinberg, Mechanism of elastic instability in Couette flow of polymer solutions : experiment, Phys. Fluids **10** (1998) 2451–2463.

[5] B. Alibenyahia, C. Lemaitre, C. Nouar and N. Ait-Messaoudene, Revisiting the stability of circular Couette flow of shear-thinning fluids, J. Non-Newt. Fluid Mech. **183–184** (2012) 37–51.

[6] C. A. Jones, The transition to wavy Taylor vortices, J. Fluid Mech. **157** (1985) 135–162.

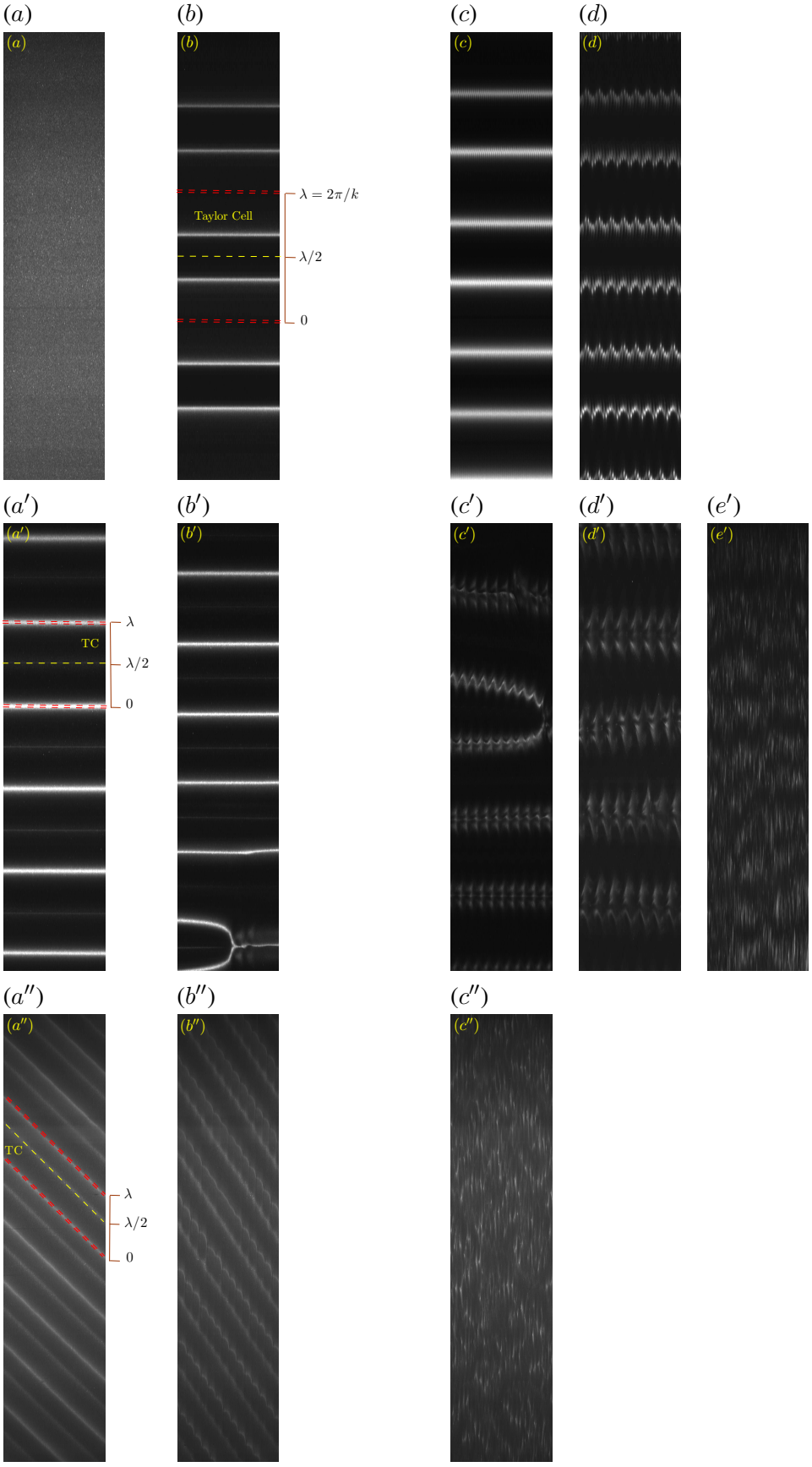

FIGURE 5: Space-time diagram of distinct flow patterns :
- 80 wt% glycerol solution : a)laminar, b)$2Re_c$, c)$7.3Re_c$, d)$10.7Re_c$,
- 0.1 wt% xanthan gum : a′)$1.5Re_c$, b′)$1.75Re_c$, c′)$1.85Re_c$, d′)$2.5Re_c$, e′)$5Re_c$
- 0.5 wt% xanthan gum : a″)$1.1Re_c$, b″)$1.2Re_c$, c″)$1.5Re_c$.

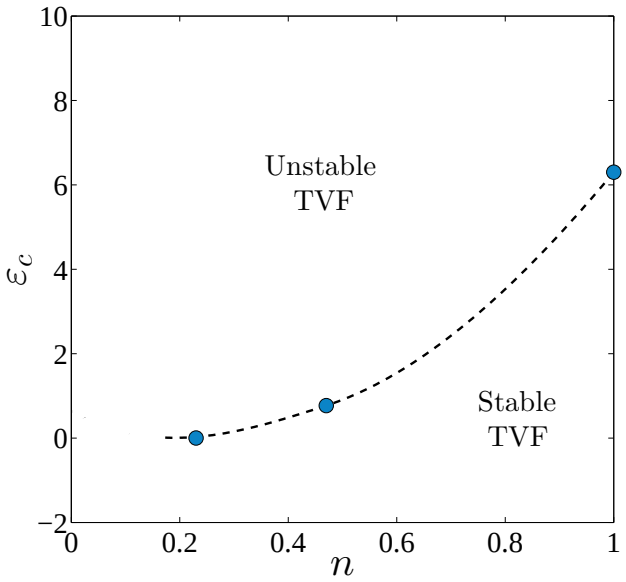

FIGURE 6: TVF instability diagram *vs* shear-thinning effects n : (filled circle) experiment data and (dashed line) guide of eyes.

[7] H. Fasel and O. Booz, Numerical investigation of supercritical Taylor-vortex flow for a wide gap, J. Fluid Mech. **138** (1984) 21–52.

[8] J. E. Burkhalter and E. L. Koschmieder, Steady supercritical Taylor vortex flow, J. Fluid Mech. **58** (1973) 547–560.

[9] M.P. Escudier, I. W. Gouldson, D. M. Jones, Taylor vortices in Newtonian and shear-thinning liquids, Proc. R. Soc. Lond. A. **449** (1995) 155–176.